Calculated and measured effects of bearing faults in elliptically deformed ball bearings

Adam Skowronek[1], Karsten Moritz[2], Joachim Bös[2], and Tobias Melz[2,3]

[1] *TU Darmstadt, Fachgebiet Systemzuverlässigkeit und Maschinenakustik SzM, former employee, email: adam.skowronek1@gmail.com*

[2] *TU Darmstadt, Fachgebiet Systemzuverlässigkeit und Maschinenakustik SzM, 64289 Darmstadt, Germany*

[3] *Fraunhofer-Institut für Betriebsfestigkeit und Systemzuverlässigkeit LBF, 64289 Darmstadt, Germany*

Introduction

Provided that the bearing rings stay in a cylindrical shape during operation, the load distribution and the vibration excitation in bearings can be calculated [1, 2]. However, bearings in strain wave gearings undergo a rotating elliptic deformation and, therefore, this assumption cannot be made. In previous papers, a model for the calculation of the deformations and forces in these bearings as well as some simulation results were presented [3, 4]. In the present study, the model is used to analyze the effects of bearing faults on the radial movement of the outer ring. The calculations as well as measurements from a test stand show that faults on different bearing parts can be distinctly identified by evaluating envelope spectra.

Strain wave gearings

A schematic diagram of a strain wave gearing is shown in Figure 1. An inelastic elliptic disk (input shaft, pos. 1) deforms a bearing (pos. 2) as well as a pan with external teeth (output shaft, pos. 3), which hence engage the internal teeth of a rigid hollow wheel (pos. 4). Due to slightly differing numbers of teeth, the pan rotates slowly when the elliptic disk is driven, causing high transmission ratios between disk and pan of up to 300:1 in one stage.

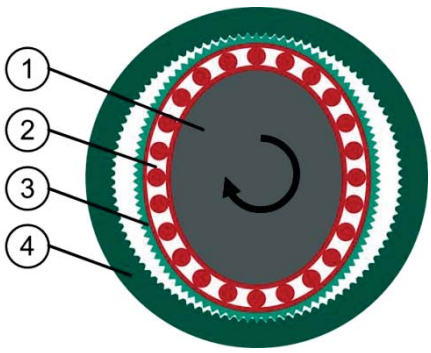

Figure 1: strain wave gearing

Model description

The model has been explained in more detail in a previous paper [3] and is described only briefly in the following.

The ball contact forces are modeled as radial point forces applied to the outer bearing ring, deforming the ring and the pan elastically. Based on finite element simulations the compliance matrix $\underline{H}$ between the ring deformations in the contact points $\underline{u}$ and the contact forces $\underline{F}$ is established. Given a known geometry of the disk and the balls, the loads necessary for the corresponding ring deformation can be calculated according to

$$\underline{F} = \underline{H}^{-1} \cdot \underline{u}. \quad (1)$$

In addition to this equation, an iteration procedure is used to consider non-linear behavior caused by the contact between the balls and the races (Hertzian stress and no drag forces). By calculating the forces and deformations in various angle positions of the disk, the model simulates the course of these data during the rotation of the input shaft. In this study, the model also includes faults on the inner ring, on the outer ring, and on a ball of the bearing. They are represented by point-shaped irregularities on these parts with an extent of 2 µm. For the assessment of the vibration excitation, the calculated radial acceleration at a point on the outer ring is evaluated in the time and frequency domain.

Measurement setup

The tested bearings are mounted in a reduced strain wave gearing. That means they are strained between an elliptic disk and an elastic pan, which, thus, is deformed elliptically. In a test stand the disk is rotating with 1000 rpm, deforming the outer ring and the stationary pan continuously. During the rotation, a sensor records the radial acceleration on the elastic pan (see Figure 2), which can be compared with the calculated data from the model. To acquire reliable test data initial measurements are conducted with 9 bearings in undamaged condition and 3 tests per bearing (27 tests). Afterwards, the bearings are dismounted, and punctual deformations are driven into the surfaces of the inner rings, outer rings, and balls (see Figure 3), thus creating three bearings for each fault. Subsequently, the measurements are repeated with the damaged bearings.

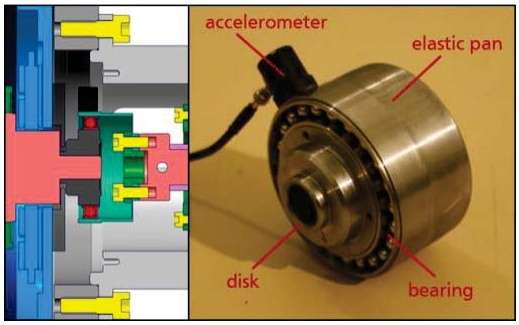

Figure 2: position of bearing and accelerometer in test stand

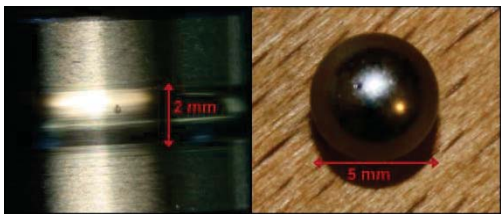

Figure 3: deformation on inner ring and on ball

Numerical results

The simulations show that even with ideal geometry (smooth surfaces, no faults) there is a chain of impulses in the calculated acceleration signal. It was shown that these results are caused by changing load conditions due to the elliptic deformation of the bearing and occur with the characteristic frequencies of the bearing, mainly with f_I (see Figure 4 and Table 1). Faults on bearing parts cause additional impulses with different patterns depending on the damaged part. The impulses take place when the faults are overrun by balls that are, at that moment, loaded with contact forces. As this is only the case in a small area of the elliptic disk (near the maximal diameter), the faults cause short chains of only 3 or 4 impulses (see Figure 5). Because of the few impulses in a row the faults are more difficult to detect than in a continuous impulse chain and have little effect on the calculated amplitude spectra. However, they can be identified by evaluation of the envelope spectra, which show a significantly higher sensitivity to impulses (Figure 6).

Table 1: characteristic bearing frequencies

frequency	calculation
rotation of cage	$f_c = 0.5 \cdot f_n \cdot (1 - D_B/D_P)$
overrun of inner ring by ball	$f_I = 0.5 \cdot f_n \cdot z \cdot (1 + D_B/D_P)$
overrun of outer ring by ball	$f_O = 0.5 \cdot f_n \cdot z \cdot (1 - D_B/D_P)$
contact of ball fault with inner/outer ring	$f_B = f_n \cdot (D_T/D_B - D_B/D_P)$
f_n: rotational frequency, D_B: ball diameter, D_P: pitch diameter, z: number of balls	

Experimental results

Like in today's tools for vibration diagnosis and due to the amount of data, the measured accelerations are analyzed automatically. Therefore, the values in the amplitude and envelope spectra at characteristic bearing frequencies are identified and compared to data without damages. The results show that, like in the simulations, the damages have no significant impact on the amplitude spectra, whereas they lead to increased values in the envelope spectra. The results, expressed in averaged multiplication factors for each damage, are shown in Table 2. For example, the envelope spectra with faults on the outer ring show a 62 times higher acceleration at f_O than the tests without faults. That way, it was possible to identify the faults and assign them to the damaged parts in all measurements.

Summary

It was shown that even in an undamaged condition elliptically deformed bearings show impulse-shaped vibration excitations. Damaged bearing parts, however, cause stronger and additional impulses, making the damages identifiable in the envelope signal by means of automatically performed vibration diagnoses.

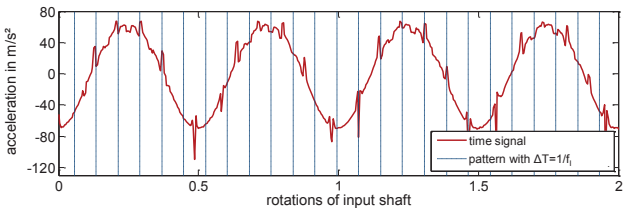

Figure 4: calculated acceleration, ideal geometry

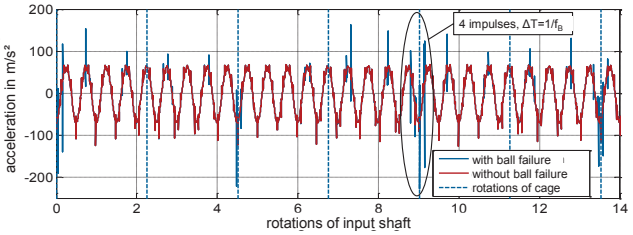

Figure 5: calculated acceleration with/without ball fault

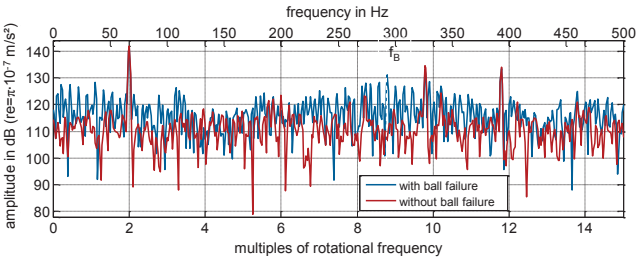

Figure 6: envelope spectrum with/without ball fault

Table 2: measured multiplication factors of accelerations

fault	spectrum	f_B	f_I	f_O	f_I+2f_n	f_O+2f_n
ball	amplitude	1.7	1.1	3.1	1.4	4.0
	envelope	**21.3**	7.1	10.6	7.7	**16.0**
inner ring	amplitude	0.6	0.7	0.7	0.8	0.8
	envelope	4.5	**17.9**	0.9	**6.0**	1.3
outer ring	amplitude	1.1	0.9	**5.2**	0.8	4.2
	envelope	3.6	4.4	**62.2**	2.2	**39.1**

References

[1] Harris, T.A., Kotzalas, M.N.: Rolling bearing analysis, 5th edition, Taylor & Francis, Boca Raton, Florida, 2006

[2] Collacott, R.A., Neale, M.J.: Mechanical fault diagnosis and condition monitoring, Chapman & Hall, London, 1977

[3] Skowronek, A., Kuhl, S., Bös, J., Hanselka, H.: Schwingungserregung in elliptisch verformten Wälzlagern, DAGA 2012, Darmstadt

[4] Skowronek, A., Kuhl, S., Bös, J., Hanelka, H.: Parameters influencing the vibration excitation in elliptically deformed ball bearings, AIA-DAGA 2013, Meran.